Soft Matter

PAPER

View Article Online
View Journal | View Issue

Published on 04 November 2019. Downloaded by Auckland University of Technology on 1/3/2020 9:51:29 AM.

Check for updates

Cite this: *Soft Matter*, 2019, **15**, 9721

# Protein-based microsphere biolasers fabricated by dehydration†

Toan Van Nguyen,[ab] Nhat Van Pham,[c] Hanh Hong Mai,[b] Dung Chi Duong,[d] Hai Hoang Le,[d] Riccardo Sapienza[e] and Van-Duong Ta*[d]

Received 9th August 2019,
Accepted 1st November 2019

DOI: 10.1039/c9sm01610d

rsc.li/soft-matter-journal

Biolasers made of biological materials have attracted considerable research attention due to their biocompatibility and biodegradability, and have the potential for biosensing and biointegration. However, the current fabrication methods of biolasers suffer from several limitations, such as complicated processing, time-consuming and environmentally unfriendly nature. In this study, a novel approach with green processes for fabricating solid-state microsphere biolasers has been demonstrated. By dehydration *via* a modified Microglassification™ technology, dye-doped bovine serum albumin (BSA) droplets could be quickly (less than 10 minutes) and easily changed into solid microspheres with diameters ranging from 10 μm to 150 μm. The size of the microspheres could be effectively controlled by changing either the concentration of the BSA solution or the diameter of the initial droplets. The fabricated microspheres could act as efficient microlasers under an optical pulse excitation. A lasing threshold of 7.8 μJ mm$^{-2}$ and a quality ($Q$) factor of about 1700 to 3100 were obtained. The size dependence of lasing characteristics was investigated, and the results showed a good agreement with whispering gallery mode (WGM) theory. Our findings contribute an effective technique for the fabrication of high-$Q$ factor microlasers that may be potential for applications in biological and chemical sensors.

## 1. Introduction

Biolasers are laser sources composed of materials of biological origin, and they have attracted considerable interest due to their potential applications in bio-integration and biosensing.[1–4] Various biological materials including poly lactic-*co*-glycolic acid, starch, protein, pectin, cellulose, and curcumin have been explored for laser microcavities.[5–9] Among them, bovine serum albumin (BSA) is considered to be an excellent biomaterial because of its biocompatibility and the ability to be transported in the human body.[10,11] Along with the developments of new materials, new lasing architectures such as random lasing,[12,13] Fabry–Perot,[14,15] distributed feedback,[16,17] and whispering gallery mode (WGM) cavities,[18–21] have been developed for biolasers. Particularly, microsphere biolasers are very interesting owing to their simple fabrication, high quality ($Q$) factor, low-lasing threshold and promising properties for ultra-sensitive biosensors with a dimension down to the intracellular level.[22,23]

Microsphere biolasers can be fabricated using several techniques such as vacuum freeze-drying,[7] slow solvent evaporation,[9] formation of oil droplets in cells,[19] emulsion and dehydration of droplets in polydimethylsiloxane (PDMS).[8] Even though the available methods are effective for making microsphere biolasers, there are still several limitations including complicated multiple fabrication processes,[7,19] environmentally unfriendly nature (using solvent)[8] and time-consuming (up to more than 12 hours).[7] As a result, a novel technique that allows microsphere biolaser fabrication in a short time (less than 10 minutes) with green processing is important for the development of biolasers.

In biology, dehydration is a common technique used for producing solid formulation of biologics. Particularly, a recently developed process, the so-called Microglassification™, is an effective method for fabricating solid microspheres rapidly and controllably from a protein solution.[24] In this technique, protein droplets can turn into solid spheres quickly by the diffusion of water molecules inside the droplet to the appropriate outer environment as decanol and pentanol until the dynamic equilibrium is established.[25] Surprisingly, the use of this approach for the fabrication of microsphere biolasers has not been explored so far. In this study, we demonstrate the

[a] *Department of Physics, Le Quy Don Technical University, Hanoi 100000, Vietnam*
[b] *Department of Quantum Optics, Faculty of Physics, VNU University of Science, Vietnam National University, Hanoi 100000, Vietnam*
[c] *Department of Advanced Material Science and Nanotechnology, University of Science and Technology Hanoi VAST, Hanoi 100000, Vietnam*
[d] *Department of Optical Devices, Le Quy Don Technical University, Hanoi 100000, Vietnam. E-mail: duong.ta@mta.edu.vn*
[e] *The Blackett Laboratory, Department of Physics, Imperial College London, London, SW7 2AZ, UK*

† Electronic supplementary information (ESI) available: Movie S1 demonstrates the formation of a solid microsphere biolaser from a droplet *via* dehydration. See DOI: 10.1039/c9sm01610d

Published on 04 November 2019. Downloaded by Auckland University of Technology on 1/3/2020 9:51:29 AM.

fabrication and optical characterizations of high-quality microsphere biolasers based on a modified Microglassification™ technology.

## 2. Experimental

### Preparation of dye-doped BSA solutions

Bovine serum albumin (BSA, ≥98% purity), Rhodamine B (RhB, ≥95% dye), and 1-decanol (the so-called decanol in short, ≥99% purity) were purchased from Sigma-Aldrich. First, BSA solutions with four different concentrations were obtained by dissolving 1 g of BSA in 1, 4, 7 and 9 mL deionized water. Subsequently, 1 mL of 1 wt% RhB aqueous solution was added to the above four BSA solutions. As a result, RhB-doped BSA solutions with BSA concentrations of 500, 200, 125 and 100 mg $mL^{-1}$ were obtained. The dry ratio of RhB to BSA in the four solutions is the same, which is 99 wt% of BSA and 1 wt% of RhB.

### Fabrication of microsphere biolasers

First, a micropipette was used to form droplets of different sizes in decanol. It should be noted that decanol was stored in a Teflon container (instead of an ordinary glass beaker) due to its hydrophobic property, which allows obtaining perfect solid microspheres. The droplets were kept in decanol until the dehydration process was completed (about 10 minutes). Then, the obtained solid microspheres (which settled down at the bottom of the container) were taken out and subsequently heated at 100 °C for 5 minutes to completely remove decanol. Finally, the microspheres were left to cool down to room temperature under ambient conditions.

### Optical characterizations

An optical microscope with a magnification of 10× and 40× equipped with a camera was used to monitor the formation of microspheres. During the dehydration process, the camera continuously captured the images of the droplets after equal intervals of 6 s. The droplet sizes were determined using the MATLAB software. In addition, the surface morphology of the microspheres was determined by SEM (TM4000plus-HITACHI). The microspheres were coated with a thin gold layer of about 10 nm thickness (by sputtering) before SEM analysis.

A micro-photoluminescence (μ-PL) setup was used to study the obtained microspheres. The pumping source is an Nd:YAG nanosecond pulse laser (Litron Lasers) with a wavelength of 532 nm, a repetition rate of 10 Hz and a pulse duration of 4–7 ns. The microspheres were excited using a focus laser beam with a spot size of ~350 μm in diameter. Emission from the microspheres was then collected using a 10× objective and subsequently delivered to an AvaSpec-2048L (Avantes) for spectral recording. The spectral resolution is ~0.2 nm. All optical characterizations were performed in air, at room temperature, and under ambient conditions.

## 3. Results and discussion

Fig. 1 shows the dehydration process starting as soon as a liquid droplet is formed inside decanol. The aqueous droplet

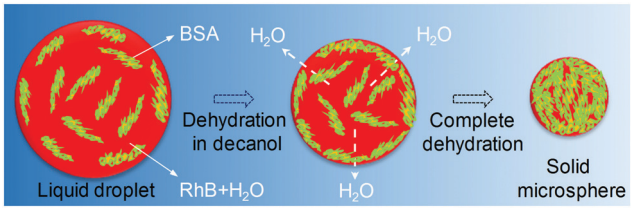


Fig. 1 Illustration of the dehydration process of a dye-doped liquid droplet in decanol.

contains BSA and Rhodamine (RhB) dye molecules. The solubility of decanol in water is very low, which allows neglecting decanol diffusion into micro-droplets.[26] However, the solubility of water into decanol is high enough to ensure that the amount of water in the droplet is much lower than the dissolution capability of the surrounding medium. Based on this effect, Rickard *et al.* and Aniket *et al.* have successfully studied the dehydration of BSA and lysozyme using a pipette technique to obtain the rigid sphere of protein.[24,25] In these studies, the system can be seen as the one-way diffusion of water into decanol, and the diffusion of protein into decanol and decanol into water can be ignored. This process is expected to be similar to the dehydration of our droplets. In addition, the RhB molecules are dissolved in decanol but the portion of RhB molecules leaking into decanol is negligible owing to the hydrophobic and electrostatic interactions of the RhB molecules with the BSA molecules.[27] The dehydration process is completed when the thermodynamic equilibrium is reached, whereas nearly all water molecules are removed from the droplets, and solid-state microspheres of dye-doped BSA are formed.[25,28]

Fig. 2 presents the optical microscope and SEM images of the dye-doped BSA microspheres. Their size can vary flexibly from 10 to 150 μm depending on the experimental conditions. In Fig. 2a, the microspheres are uniformly dark red in color. In addition, the microsphere surface is relatively smooth (Fig. 2b),

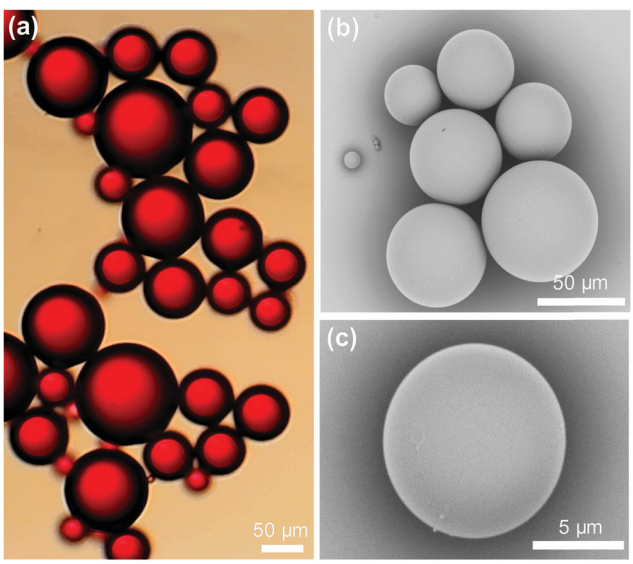


Fig. 2 (a) Optical microscope image of dye-doped BSA microspheres. (b) Scanning electron microscope (SEM) image of the BSA microspheres with different sizes. (c) High-magnification SEM image of a single microsphere.


This journal is © The Royal Society of Chemistry 2019

Published on 04 November 2019. Downloaded by Auckland University of Technology on 1/3/2020 9:51:29 AM.

which could be seen more clearly in the high-magnification SEM image of a single microsphere in Fig. 2c. The results indicated that the fabricated BSA microspheres would support strong optical confinement.

Controlling the size of microlasers is a critical task.[4] For a fixed concentration of the BSA solution, the final diameter of dye-doped BSA microspheres depends on their initial droplet size.[25,29] Fig. 3a shows the dehydration process of four different initial diameters of 100, 94, 89 and 78 μm droplets with the same initial concentration of 500 mg $mL^{-1}$. It can be seen clearly that the larger droplet size takes longer time by 350, 310, 245 and 150 seconds to complete the dehydration process, respectively. The inset in Fig. 3a represents the final diameter ($D_f$) of the microspheres after the dehydration process is correspondingly linearized with the initial diameters ($D_0$), providing a simple and effective solution to control the size of microspheres. Fig. 3b demonstrates the shrinking of droplet diameter during the dehydration process from the initial diameter reduced from 78 μm to 44.5 μm at the end of the process (ESI,† Movie S1). The result indicates that if the initial droplets (from a fixed concentration) are uniform, then solid microspheres with the same size can be obtained. Uniform droplets can be made using a microfluidic[28] or solution printing system.[30,31]

The final concentration of BSA in microspheres affects their structure. The diffusion of water leads to the reduction in the droplet size, and therefore, the concentration of BSA in the droplets increases correspondingly. At a specific time, the concentration of BSA can be calculated using the formula: $C_t = C_0 D_0^3 / D_t^3$, as shown in Fig. 3c. The four microspheres had different initial diameters, and the concentration of BSA in the spheres increased gradually from 500 mg $mL^{-1}$ to about 1138–1150 mg $mL^{-1}$ at the end of the dehydration process. This result is similar to a previously published study, with the concentration of BSA reaching 1147 ± 32 mg $mL^{-1}$.[25]

In order to control the size of microspheres, studying the effects of the initial concentration of BSA on the dehydration process is also important. Fig. 4a describes the change in the size of four droplets at the same initial diameter of 100 μm. Using different initial concentrations of BSA solutions: 500, 200, 125 and 100 mg $mL^{-1}$, four solid-state microspheres were obtained with diameters of 76, 56.5, 48 and 45.5 μm, respectively. The inset in Fig. 4a shows that the change in the ratio of $D_f$ to $D_0$ for the microspheres, which is proportional to $(C_0)^{1/3}$, perfectly fit with the theory. To obtain smaller microspheres of the same initial size of droplets by reducing the initial concentration of BSA, it takes more time to complete the dehydration process. The longest required time to form ~100 μm-diameter microspheres is about 10 minutes, which is much faster in comparison with the fabrication time of other methods such as the 12 hours by using the vacuum freeze-drying method.[7] Fig. 4b shows the increase in the concentration of BSA in the droplets during the dehydration process. From the initial concentration of BSA solutions: 500, 200, 125 and 100 mg $mL^{-1}$, the same final concentration of BSA of microspheres can reach 1132–1138 mg $mL^{-1}$. This means that the initial BSA concentration insignificantly affects the BSA concentration at the end of the dehydration process. The final concentration of microspheres depends only on the equilibrium of the system (*i.e.* the equilibrium between the inner and outer environments of the droplet). In this case, with the same outer environment as decanol, the dehydration processes with different initial conditions will always stop at the same final concentration of BSA.

The fabricated dye-doped microspheres could act as excellent lasers under optical excitation. Fig. 5a shows the schematic of the WGM in a typical microsphere. The light is trapped inside by multiple total internal reflections at the microsphere-air interface and subsequently amplified by resonant circulation, leading to laser emission. Fig. 5b presents the emission spectra from a single microsphere (47.6 μm, initial concentration of BSA is 500 mg $mL^{-1}$). It can be seen that the photoluminescence (PL) intensity increases with the increase in the pump pulse energy (PPE) of the incident laser, and lasing emission is seen when

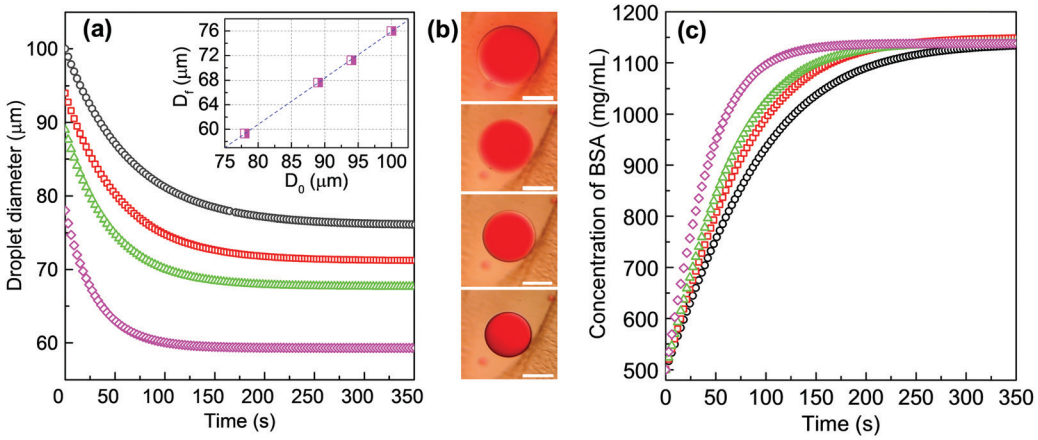


Fig. 3 (a) Dehydration process of four different dye-doped BSA droplets. The initial concentration of BSA is 500 mg $mL^{-1}$. The inset in the figure shows the relationship between the final diameter ($D_f$) of microspheres and their initial diameter ($D_0$). (b) Optical microscope images of a 78 μm-diameter BSA droplet during the dehydration process at 0, 40, 80 and 150 seconds, respectively. All scale bars are 50 μm. (c) Change of BSA concentration in the droplets during the dehydration process.

Published on 04 November 2019. Downloaded by Auckland University of Technology on 1/3/2020 9:51:29 AM.

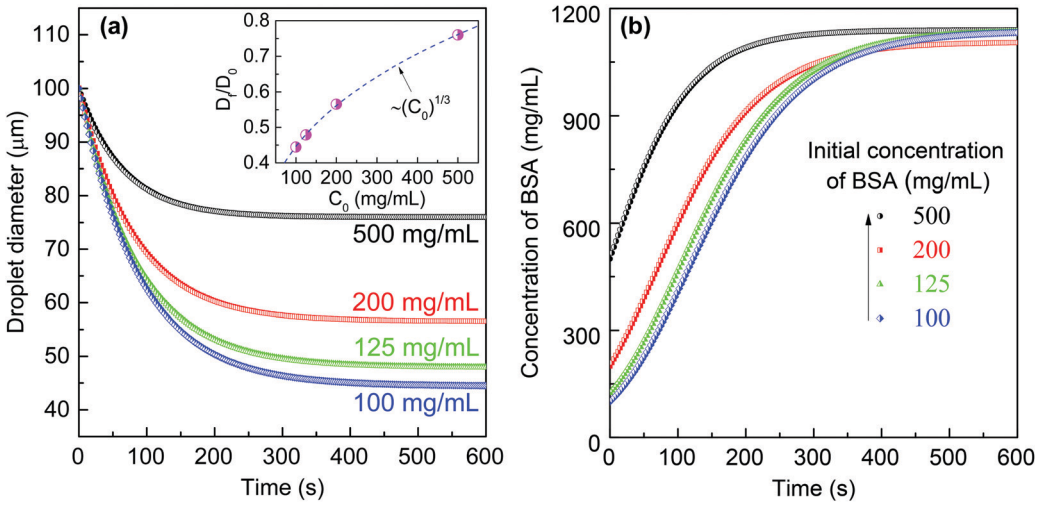


Fig. 4 (a) Dehydration process of four BSA droplets with different concentrations. The initial diameters of the droplets are similar and approximately 100 μm. The inset in figure shows the ratio of the final diameter and the initial diameter of the droplets ($D_f/D_0$) as a function of the initial BSA concentration. (b) Change in the BSA concentration of droplets with different initial concentrations.

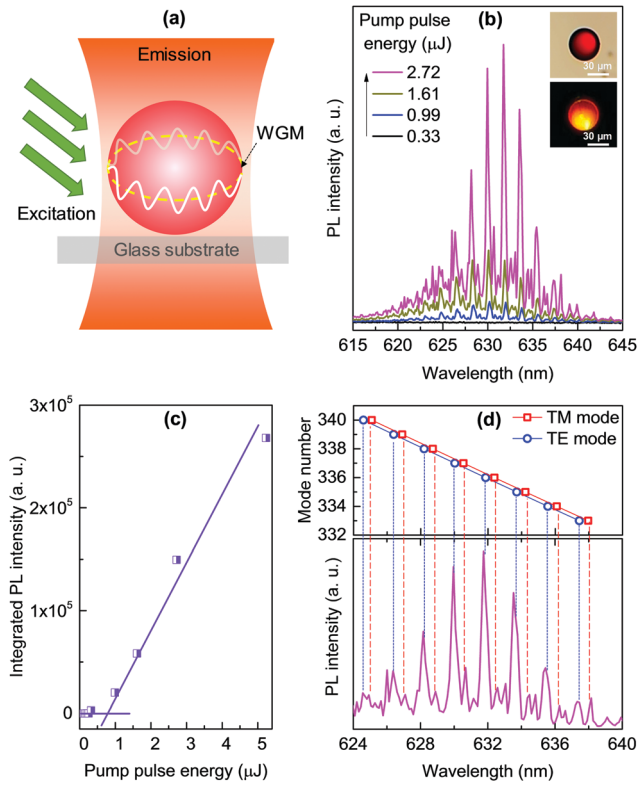


Fig. 5 (a) Schematic of the whispering gallery mode (WGM) in a microsphere. (b) Emission spectra of a 47.6 μm-diameter dye-doped BSA microsphere under pulse excitation. (c) The corresponding integrated PL intensity as a function pump pulse energy. (d) Matching between calculated lasing modes and experimental lasing wavelengths.

PPE = 0.99 μJ per pulse. The lasing modes are well recognized above the fluorescence background, with sharp peaks appearing clearly in the wavelength range from 615 to 645 nm. Besides, the integrated PL intensity is shown in Fig. 5c. A nonlinear increase in the emission intensity supports the lasing action, indicating a lasing threshold of about 0.75 μJ. The threshold is equivalent to 7.8 μJ mm$^{-2}$, which is comparable with the previous report (same material and shape),[8] and about two orders of magnitude smaller than that for starch-based biolasers.[7] Lasing modes can be well explained by the WGM theory, in particular, by using the explicit asymptotic formula.[32] By assuming the diameter of the sphere is $D$ = 47.595 μm, the mode number of the transverse electric (TE) and transverse magnetic (TM) modes are calculated to be 333 to 340, which fit very well with the experimental measurements (Fig. 5d).

The size-dependent lasing spectra of WGM lasers were studied, and the results are shown in Fig. 6. Fig. 6a–d plot the lasing spectra of four different microspheres. It can be seen that the free spectral range (FSR) decreases with the increase in the microsphere diameter. It is understandable because the FSR of a WGM laser can be determined as FSR = $\lambda^2/\pi nD$, where $\lambda$ is the lasing wavelength, and $n$ and $D$ are the refractive index and diameter of the microsphere, respectively.[33] The FSR of a 32 μm-diameter microsphere is determined to be 2.5 nm (Fig. 6a). Considering the resonant wavelength $\lambda$ = 623 nm and refractive index $n$ = 1.47, then the calculated FSR is 2.6 nm, which is very close to the experimental observation. When the size of the laser increases, its FSR decreases correspondingly. The FSR of a 123 μm-diameter microsphere is 0.7 nm (Fig. 6d), which again agrees well with the calculation assuming $\lambda$ = 630 nm. From the above equation, the FSR of various microspheres is expected to be linear with the inverse of the microsphere diameters. As shown in Fig. 6e, we experimentally obtained this linear relationship by measuring the FSR of 21 microspheres with diameters ranging from 24 to 128 μm. The result further confirms the WGM mechanism for laser action in the microspheres.

In addition to the lasing spectrum, the $Q$ factor is also expected to be dependent on the microsphere size. Fig. 7a and b show the profile of a typical lasing mode in the range of 1 nm of two

 This journal is © The Royal Society of Chemistry 2019

Published on 04 November 2019. Downloaded by Auckland University of Technology on 1/3/2020 9:51:29 AM.

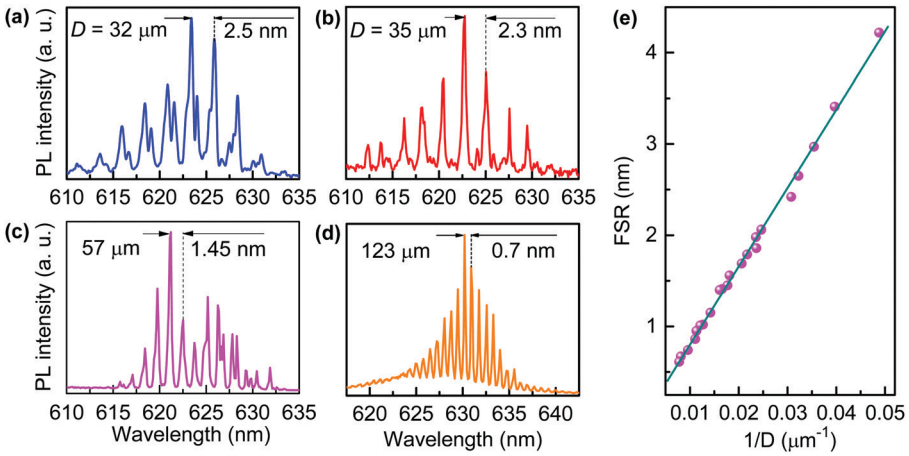


Fig. 6 (a)–(d) Emission spectra of four different dye-doped BSA microspheres with increasing diameter. (e) Experimental free spectral range (FSR) of microsphere biolasers *versus* their inverse diameters. The line is the theoretical calculation using equation FSR = $\lambda^2/\pi nD$, where $\lambda$ = 625 nm.

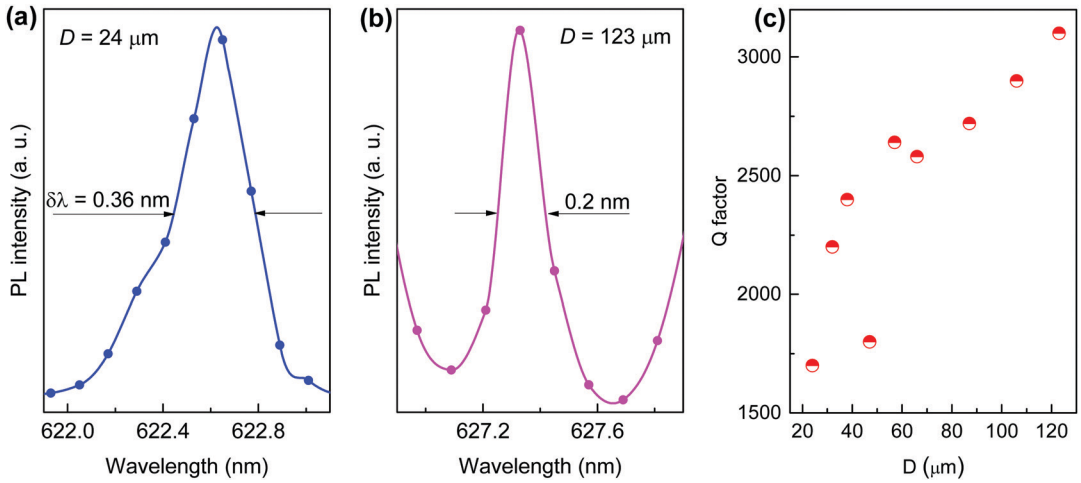


Fig. 7 (a) and (b) Full width at half maximum ($\delta\lambda$) of a 24 μm-diameter and a 123 μm-diameter microspheres, respectively. (c) *Q* factor as a function of microsphere diameter.

different microspheres. It can be seen that the spectral linewidth or the full width at half maximum ($\delta\lambda$) of a 24 μm-diameter microsphere is 0.36 nm, which nearly doubles compared with that of 0.2 nm of a 123 μm-diameter microsphere. It means that a larger microsphere exhibits narrower lasing modes compared with a smaller one. In addition, the *Q* factor of a lasing mode can be defined as $Q = \lambda/\delta\lambda$. As a result, the *Q* factor of microspheres should increase with their sizes. Indeed, we obtained a *Q* factor of about 1700 for a 24 μm-diameter microsphere and 3100 for a 123 μm-diameter microsphere. Fig. 7c indicates that the *Q* factor is found to increase with the microsphere diameter. This effect has been previously observed and well-explained.[34] In addition, the *Q* factor of our microsphere biolasers (about 1700 to 3100) is comparable with protein-based microsphere[8] and microdisk[18] lasers fabricated using different methods. In comparison with microlasers using other materials, such as starch-based microlasers,[7] the *Q* factor of our lasers is about 2 times higher. The lower *Q* factor of the starch-based laser may be due to its unusual ellipsoid shape (rather than a sphere), which does not effectively confine light.

It is noted that all the lasing properties were measured in air. Previous reports have demonstrated that BSA-based microlasers can work efficiently in an aqueous environment.[8,18] However, in this study, we have found that our microlasers tend to swell in water. This issue may be solved by annealing the microlasers at high temperature (around 100 °C), and we will investigate this in future studies.

## 4. Conclusions

We have demonstrated a green and fast process for fabricating solid-state dye-doped BSA microsphere biolasers. The technique is based on the dehydration process *via* a modified Microglassification™ technology. Our approach can produce perfect microspheres within 5–10 minutes, and is about two orders of magnitude faster when compared with the vacuum freeze-drying method. The sizes of microcavity can be tuned flexibly from 10 to 150 μm by changing the initial BSA concentration or

Published on 04 November 2019. Downloaded by Auckland University of Technology on 1/3/2020 9:51:29 AM.

initial diameter of droplets. WGM lasing emission with a lasing threshold of about 8 μJ mm$^{-2}$ and a $Q$ factor of 1700 to 3100 was obtained from the dye-doped microspheres. Lasing mechanism and size dependence of lasing characteristics were investigated, showing an agreement between experimental observation and theoretical calculation. Simple fabrication procedures and fast processing facilitate the mass production of microsphere biolasers, which may allow their practical applications in biosensing and bioimaging.

## Conflicts of interest

There are no conflicts to declare.

## Acknowledgements

This research is funded by Vietnam National Foundation for Science and Technology Development (NAFOSTED) under grant number 103.03-2017.318.

## References

1 X. Fan and S.-H. Yun, *Nat. Methods*, 2014, **11**, 141–147.
2 Y.-C. Chen and X. Fan, *Adv. Opt. Mater.*, 2019, **7**, 1900377.
3 A. J. C. Kuehne and M. C. Gather, *Chem. Rev.*, 2016, **116**, 12823–12864.
4 V. D. Ta, Y. Wang and H. Sun, *Adv. Opt. Mater.*, 2019, **7**, 1900057.
5 M. Humar, A. Dobravec, X. Zhao and S. H. Yun, *Optica*, 2017, **4**, 1080–1085.
6 I. B. Dogru, K. Min, M. Umar, H. Bahmani Jalali, E. Begar, D. Conkar, E. N. Firat Karalar, S. Kim and S. Nizamoglu, *Appl. Phys. Lett.*, 2017, **111**, 231103.
7 Y. Wei, X. Lin, C. Wei, W. Zhang, Y. Yan and Y. S. Zhao, *ACS Nano*, 2017, **11**, 597–602.
8 V. D. Ta, S. Caixeiro, F. M. Fernandes and R. Sapienza, *Adv. Opt. Mater.*, 2017, **5**, 1601022.
9 D. Venkatakrishnarao, M. A. Mohiddon and R. Chandrasekar, *Adv. Opt. Mater.*, 2017, **5**, 1600613.
10 F. Kratz, *J. Controlled Release*, 2008, **132**, 171–183.
11 A. Ding, L. Teng, Y. Zhou, P. Chen and W. Nie, *Polym. Bull.*, 2018, **75**, 2917–2931.
12 S. Caixeiro, M. Gaio, B. Marelli, F. G. Omenetto and R. Sapienza, *Adv. Opt. Mater.*, 2016, **4**, 998–1003.
13 Q. Song, S. Xiao, Z. Xu, J. Liu, X. Sun, V. Drachev, V. M. Shalaev, O. Akkus and Y. L. Kim, *Opt. Lett.*, 2010, **35**, 1425–1427.
14 M. C. Gather and S. H. Yun, *Nat. Photonics*, 2011, **5**, 406–410.
15 M. C. Gather and S. H. Yun, *Opt. Lett.*, 2011, **36**, 3299–3301.
16 Y. Choi, H. Jeon and S. Kim, *Lab Chip*, 2015, **15**, 642–645.
17 C. Vannahme, F. Maier-Flaig, U. Lemmer and A. Kristensen, *Lab Chip*, 2013, **13**, 2675–2678.
18 Y.-L. Sun, Z.-S. Hou, S.-M. Sun, B.-Y. Zheng, J.-F. Ku, W.-F. Dong, Q.-D. Chen and H.-B. Sun, *Sci. Rep.*, 2015, **5**, 12852.
19 M. Humar and S. Hyun Yun, *Nat. Photonics*, 2015, **9**, 572–576.
20 S. Nizamoglu, M. C. Gather and S. H. Yun, *Adv. Mater.*, 2013, **25**, 5943–5947.
21 Y.-C. Chen, Q. Chen and X. Fan, *Optica*, 2016, **3**, 809–815.
22 G. C. Righini and S. Soria, *Sensors*, 2016, **16**, 905.
23 M. R. Foreman, J. D. Swaim and F. Vollmer, *Adv. Opt. Photonics*, 2015, **7**, 168–240.
24 D. L. Rickard, P. B. Duncan and D. Needham, *Biophys. J.*, 2010, **98**, 1075–1084.
25 Aniket, D. A. Gaul, D. L. Rickard and D. Needham, *J. Pharm. Sci.*, 2014, **103**, 810–820.
26 N. Šegatin and C. Klofutar, *Monatsh. Chem.*, 2004, **135**, 241–248.
27 H.-H. Cai, X. Zhong, P.-H. Yang, W. Wei, J. Chen and J. Cai, *Colloids Surf., A*, 2010, **372**, 35–40.
28 K. Kinoshita, E. Parra, A. Hussein, A. Utoft, P. Walke, R. de Bruijn and D. Needham, *Processes*, 2016, **4**, 49.
29 M. S. P. P. S. Epstein, *J. Chem. Phys.*, 1950, **18**, 1505–1509.
30 W. Zhang, J. Yao and Y. S. Zhao, *Acc. Chem. Res.*, 2016, **49**, 1691–1700.
31 V. D. Ta, S. Yang, Y. Wang, Y. Gao, T. He, R. Chen, H. V. Demir and H. Sun, *Appl. Phys. Lett.*, 2015, **107**, 221103.
32 C. C. Lam, P. T. Leung and K. Young, *J. Opt. Soc. Am. B*, 1992, **9**, 1585–1592.
33 C. Wei, Y. Du, Y. Liu, X. Lin, C. Zhang, J. Yao and Y. S. Zhao, *J. Am. Chem. Soc.*, 2019, **141**, 5116–5120.
34 V. D. Ta, R. Chen and H. D. Sun, *Adv. Mater.*, 2012, **24**, OP60–OP64.

 This journal is © The Royal Society of Chemistry 2019